Supporting Information

Novel Cs-based upconversion nanoparticles as dual-modal CT and UCL imaging agents for chemo-photothermal synergistic therapy

Yuxin Liu †, Luoyuan Li †, QuanweiGuo, Lu Wang, Dongdong Liu, Ziwei Wei, Jing Zhou*

† These authors contribute equally in this work.

Department of Chemistry, Capital Normal University, No.105 Xi San Huan Road, Beijing 100048, P. R. China.

E-mail: jingzhou@cnu.edu.cn (J. Zhou)

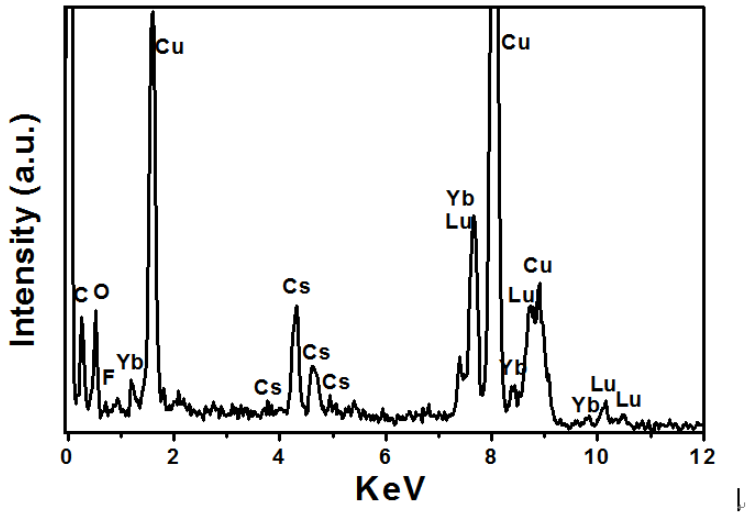

Figure S1. EDXA of UCNP-OA. Minor doped ion of Er^{3+} and Tm^{3+} cannot be found due to their low content. The presence of Cu element results from copper grid during TEM measurements.

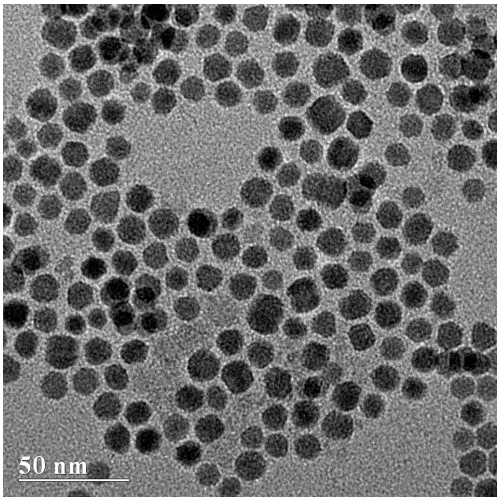

Figure S2. TEM images of the UCNP-PEG samples.

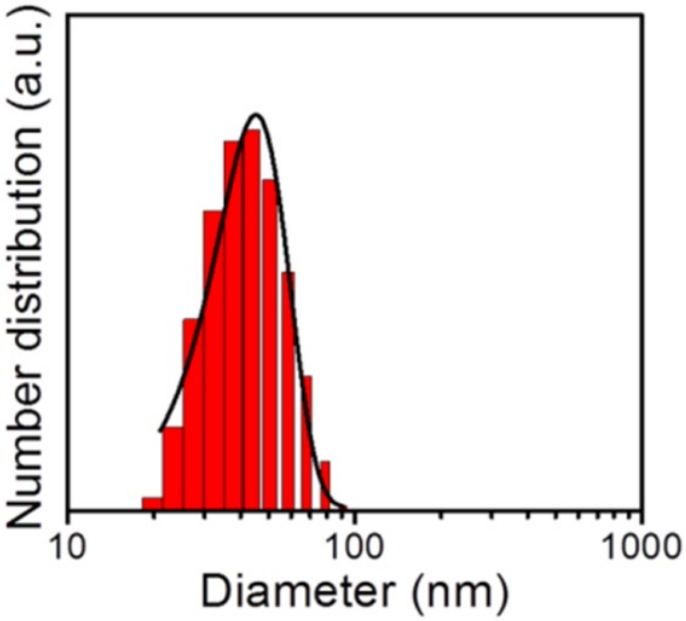

Figure S3. Hydrodynamic diameter of the UCNP-PEG.

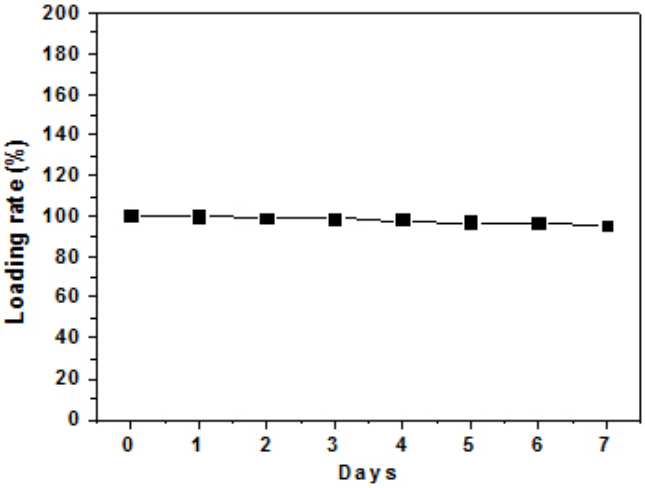

Figure S4. The loading rate of ICG within 7 days.

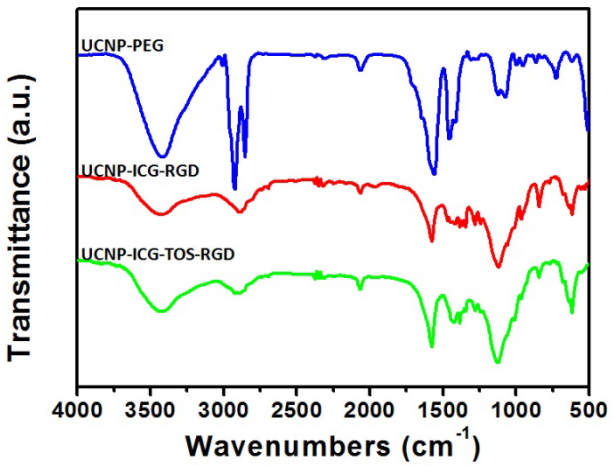

Figure S5. The FTIR spectra of UCNP-PEG, UCNP-ICG-RGD, and UCNP-ICG-TOS-RGD.

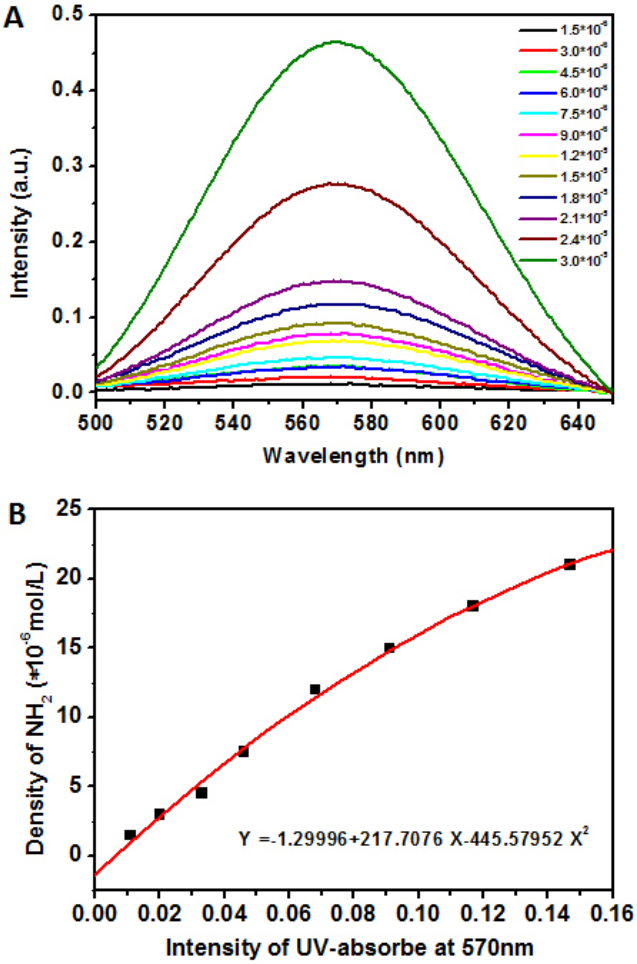

Figure S6. A) Ninhydrin method for the quantitative analysis of NH_2. B) NH_2 concentration *vs* absorption at λ = 570 nm.

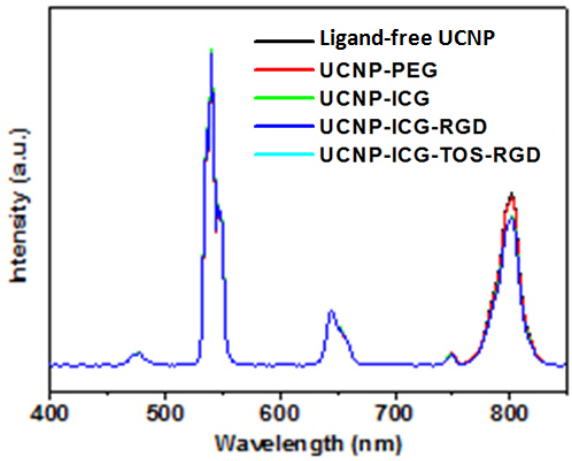

Figure S7. The UCL spectra before and after surface modification.

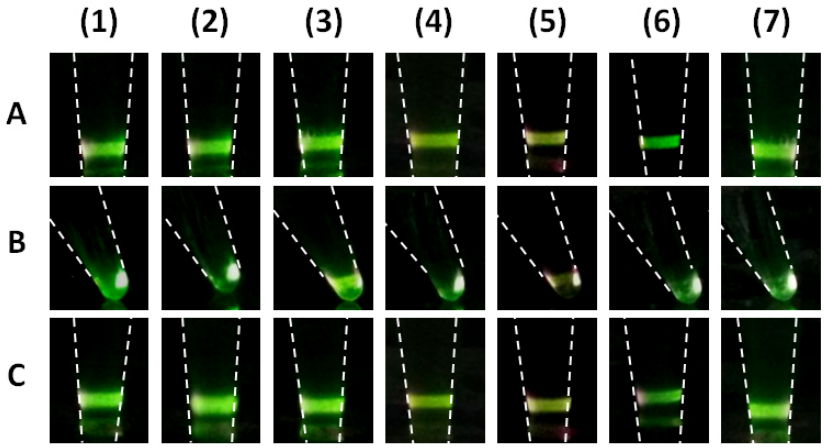

Figure S8. UCL images of the UCNP-ICG-RGD dissolved in various solutions before (A), after (B) centrifugation, and redispersion in solutions being ultrasonically treated: (1) water, (2) phosphate buffered saline (PBS), (3) 5% glucose solution, (4) fatal bovine serum (FBS), (5) Dulbecco's modified Eagle medium (DMEM), (6) 0.9% NaCl solution, and (7) artificial cerebrospinal fluid.

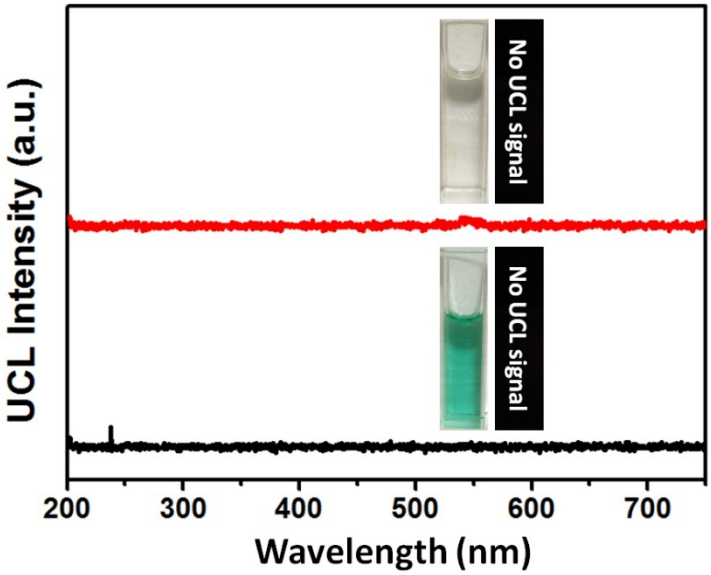

Figure S9. UCL spectra of water (A) and free ICG solution (B). Inset: photographs and UCL images of water and free ICG solution.

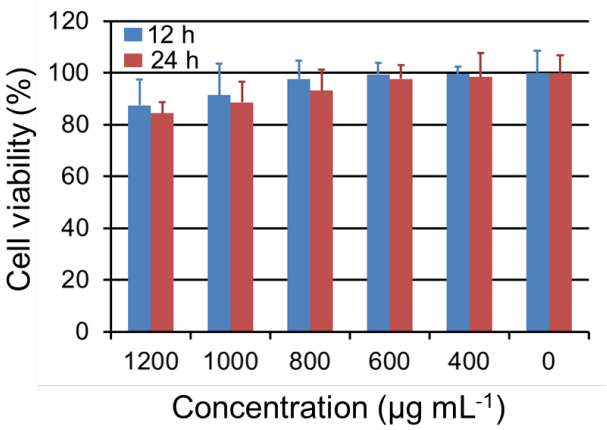

Figure S10. MTT assays of U87MG cells viability after incubating with UCNP-ICG-RGD at different concentrations for 12 h and 24 h.

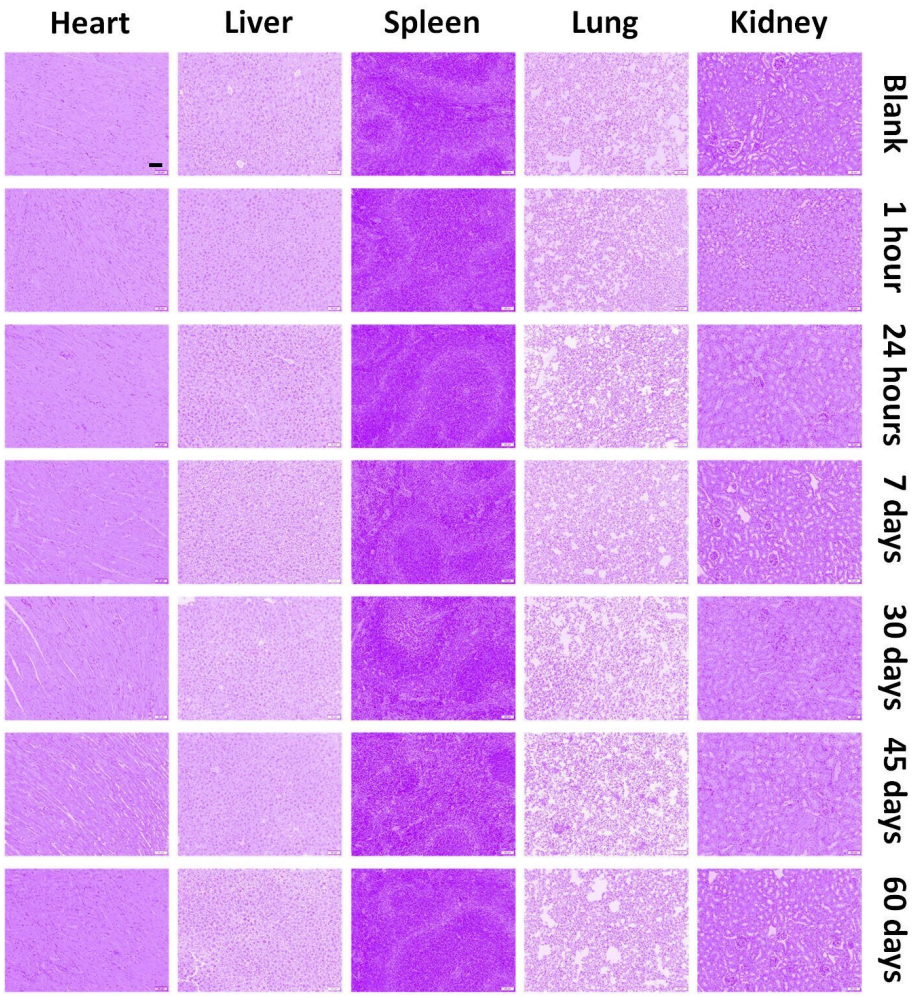

Figure S11. H&E stained images of organs, including (A) heart, (B) liver, (C) spleen, (D) lung, and (E) kidneys from mice with intravenous injections of UCNP-ICG-RGD at different time intervals (30 min, 24 h, 7 d, 30 d, 45 d, and 60 d). Scale bar: 200 μm.

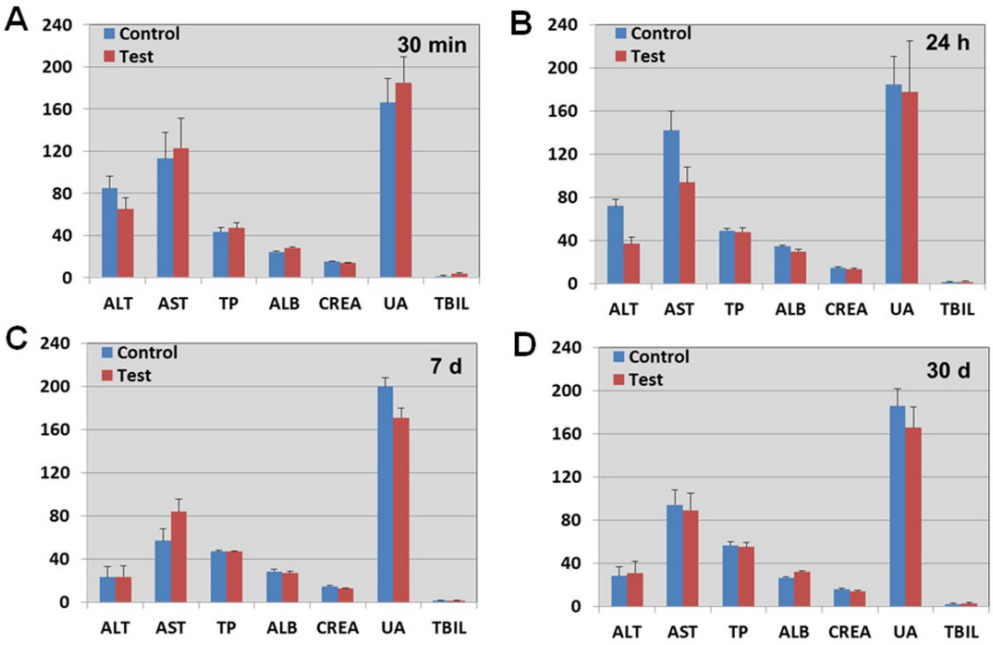

Figure S12. Hematology studies of test and control groups of nude mice (n = 5) intravenously injected with UCNP-ICG-RGD and sacrificed at (A) 30 min, (B) 24 h, (C) 7 days, and (D) 30 days. Blood index including: three important hepatic indicators (ALT (IU L^{-1}), AST (IU L^{-1}), TBIL (umol L^{-1}), TP (g L^{-1}), ALB (g L^{-1})) and two indicators for kidney functions (CREA (umol L^{-1}), UA (umol L^{-1})).

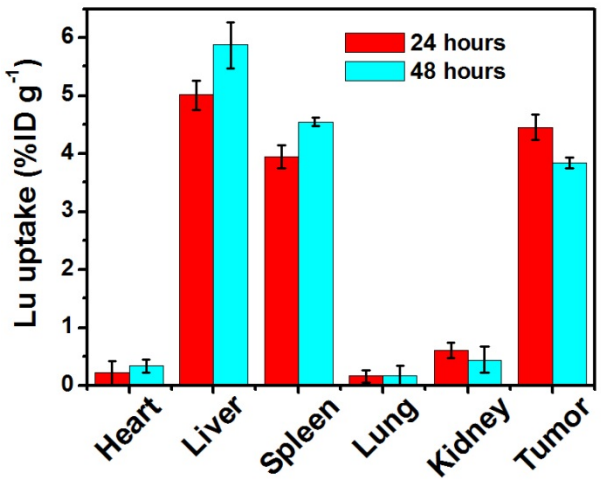

Figure S13. Inductively coupled plasma mass spectrometry (ICP-MS) analysis of biodistribution of nanoparticles (Lu^{3+} uptake%) in various organs of mice after 24 h and 48 h intravenous injection with UCNP-ICG-RGD. The major organs: (1) lung; (2) kidneys; (3) heart; (4) liver; (5) spleen; (6) tumor.

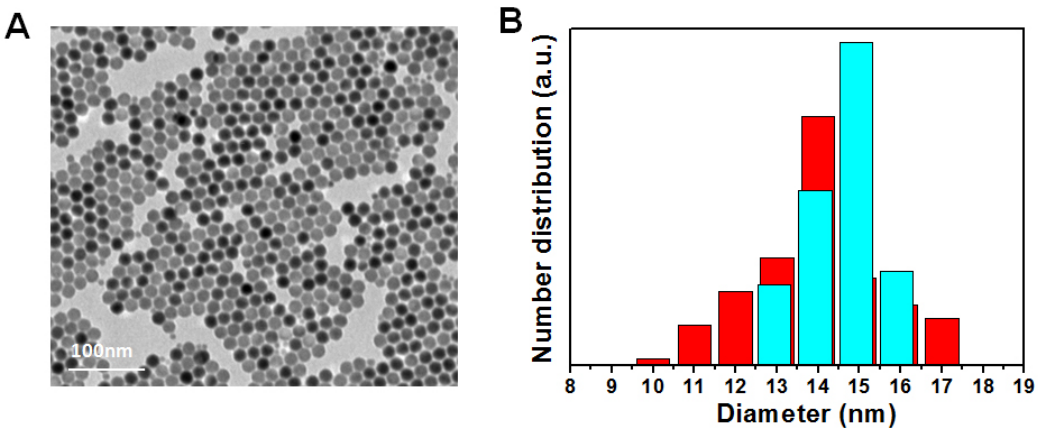

Figure S14. (A) TEM images of the $NaLuF_4$. Scale bar: 100 nm. (B) Diameter distribution of $NaLuF_4$-OA in cyclohexane (Blue) compared with UCNP-OA (Red).

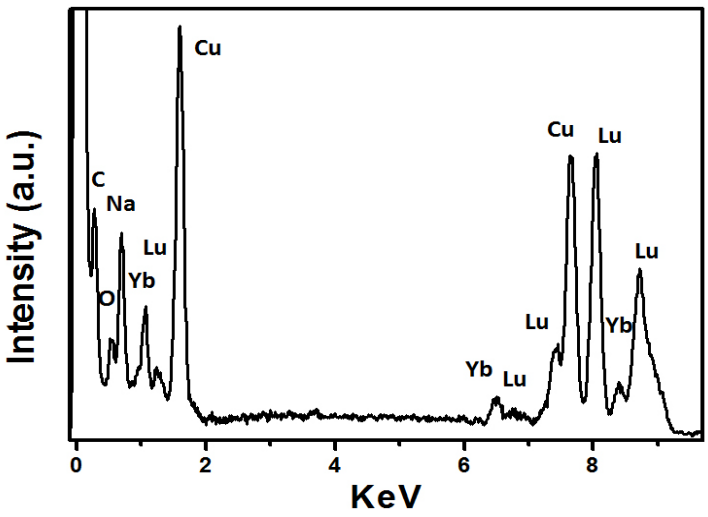

Figure S15. EDXA of $NaLuF_4$-based nanoparticles. Minor doped ion of Er^{3+} and Tm^{3+} could not be found due to their low content. The presence of Cu element results from copper grid during TEM measurements.

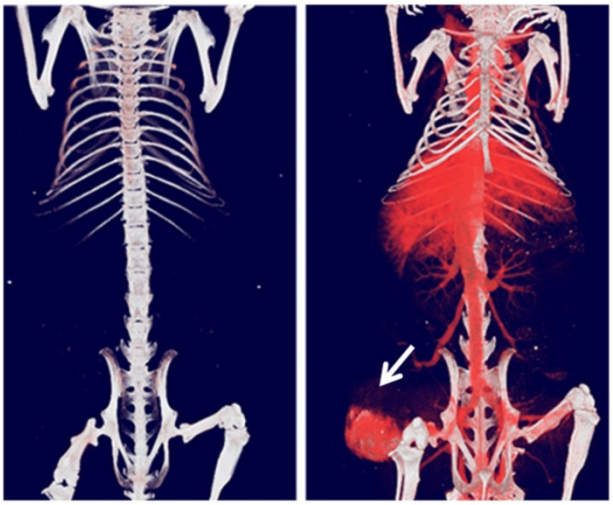

Figure S16. 3D CT volume-rendered images of mice were obtained before the intravenous injection (left), 30 min after the injection (right) of UCNP-ICG-RGD (200 μL, 1 mg mL^{-1}). White arrows indicated the locations of the tumors.

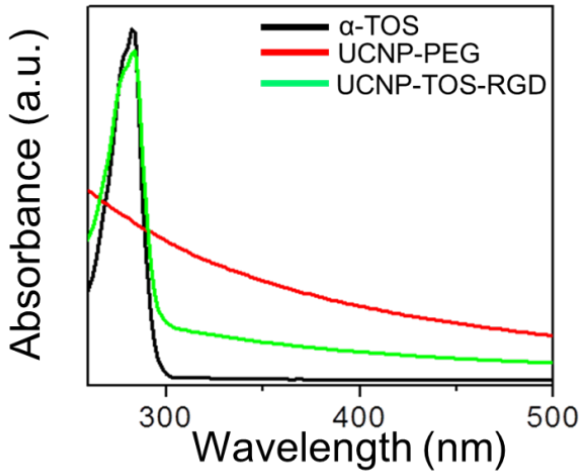

Figure S17. The UV-vis-NIR spectra of free *α*-TOS, UCNP-PEG, and UCNP-TOS-RGD.

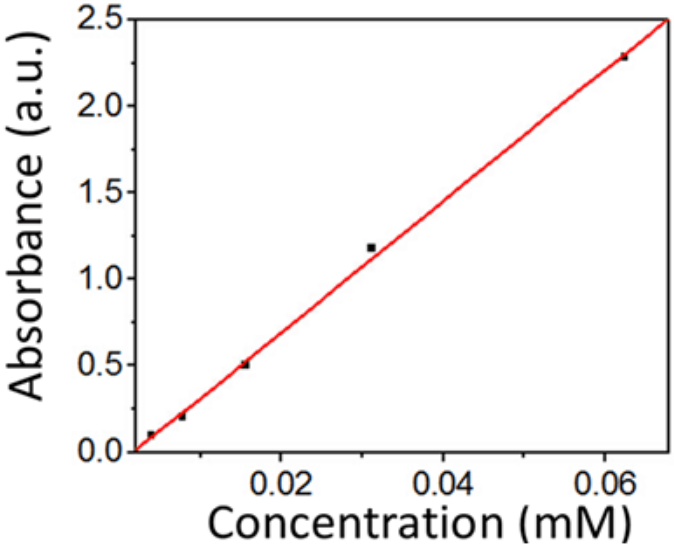

Figure S18. Absorption at λ = 785 nm *vs* ICG concentration.

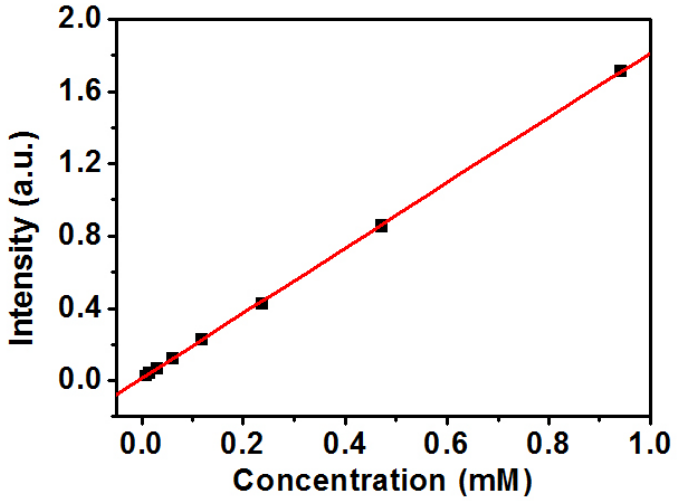

Figure S19. Absorption at λ = 284 nm*vs*α-TOS concentration.

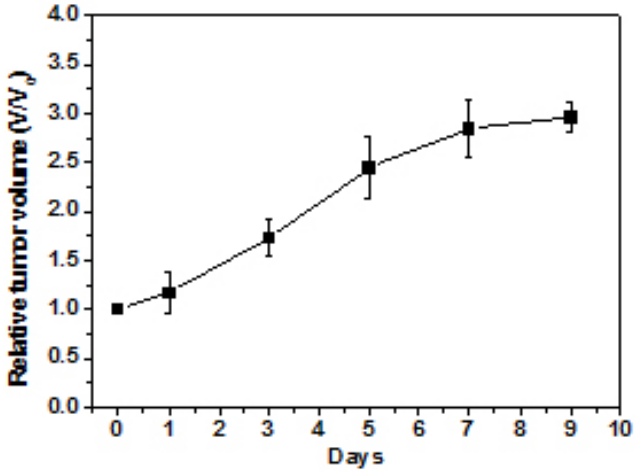

Figure S20. Growth rate of mice following intravenous injection with 200 μL fresh medium (Blank group).

Table S1. Biodistribution of nanoparticles (relative Lu uptake expressed by tumor-to-organ ratio) 24 h after intravenous injection with UCNP-PEG, UCNP-ICG, and UCNP-ICG-RGD.

	Relative Lu uptake (tumor-to-organ ratio)		
	UCNP	UCNP-ICG	UCNP-ICG-RGD
Tumor	1.00	1.00	1.00
Heart	11.43	9.20	20.39
Liver	0.17	0.09	0.89
Spleen	0.48	1.12	1.13
Lung	16.77	14.80	27.9
kidney	5.12	5.34	7.40

Table S2. Comparison of the CT value between the previously reported CT contrast agents and the $CsLu_2F_7$-based nanomaterials in this study. The HU value of the $CsLu_2F_7$-based nanoparticles at 10 mg mL^{-1} was up to 232.2 which was superior to that of reported CT contrast agents (HU =138 for $NaGdF_4$), even for $NaLuF_4$-based nanoparticles (HU = 176.3-220) at the same mass concentration.

Nanomaterial	Diameter (nm)	Concentration (mg mL^{-1})	CT Value (HU)	Reference
$NaGdF_4$:Yb,Er	5	10	138	*Adv. Funct. Mater.* 2011; 21: 4470-7
$NaLuF_4$:Yb, Er	17	10	182.6	*Theranostics* 2013; 3: 346-53
$NaLuF_4$:Yb, Tm@SiO_2 -GdDTPA	30	10	220	*Biomaterials* 2012; 33: 5394-405
$NaLuF_4$:Yb, Er, Tm	13-16	10	176.3	In this work
$CsLu_2F_7$:Yb, Er, Tm	10-17	10	232.2	In this work

Table S3. Comparison of CT values between the $NaLuF_4$- and $CsLu_2F_7$-based nanoparticles at same mole concentration.

CT Value (HU)	Lu Concentration (mM)		
	9	18	36
$NaLuF_4$:Yb, Er, Tm (13-16 nm)	34.4	70.2	174.5
$CsLu_2F_7$:Yb, Er, Tm (10-17 nm)	51.7	114.6	250.3